2018 Annual American Control Conference (ACC)
June 27–29, 2018. Wisconsin Center, Milwaukee, USA

Output Feedback Trajectory Tracking Control via Uncertainty and Disturbance Estimator

Jiguo Dai, Beibei Ren, and Qing-Chang Zhong

***Abstract*—This paper proposes an output feedback trajectory tracking control based on the uncertainty and disturbance estimator (UDE) technique. The studied nonlinear system is single-input-single-output (SISO), bounded-input-bounded-output (BIBO), and Lipschitz smooth. The main idea is that the nonlinear system is firstly approximated by a proper first-order linear system plus a lumped uncertainty term, which is estimated and compensated through the UDE. The proposed control technique is modeling-free, and only uses the information of system output and the spectrum of the lumped uncertainty term. It also relaxes the structural constraint in the conventional UDE-based robust control. In order to improve the tracking performance, the internal model principle is adopted in the design of the filter in the UDE. The proposed control design is successfully applied to the position control of a piezoelectric nanopositioning system with hysteresis nonlinearity. The experimental results show that the piezoelectric stage can achieve a fine tracking at $1100Hz$, which is 37.93% of the lowest resonant frequency, a significant improvement compared to the commercially available range at $1\% - 10\%$.**

I. Introduction

In recent years, robust control design has received a lot of attention in control community. Among different robust control approaches, the UDE-based robust control, proposed in [1], has a simple structure with strong robustness. This approach has been successfully applied into different applications [2], [3], [4], [5], [6], [7], [8], [9]. The UDE-based robust control uses a proper filter to estimate and compensate the lumped uncertainty (total effect of the uncertainties and disturbances in the system). As disclosed in [10], this approach has two degrees of freedom, which are, the design of the reference model (to achieve a desired tracking performance), and the design of a low-pass filter (to attenuate the effect of uncertainties and disturbances). A systematic design principle for this approach is investigated in [11], and asymptotic performance is achieved by applying the internal model principle [12]. However, the conventional UDE-based robust control is still facing two gaps between its theory and applications.

This work was supported by the National Science Foundation under Grant CMMI-1728255.

Jiguo Dai and Beibei Ren are with the Department of Mechanical Engineering, Texas Tech University, Lubbock, 79409-1021, USA. (e-mail: jiguo.dai@ttu.edu, beibei.ren@ttu.edu).

Qing-Chang Zhong is with the Department of Electrical and Computer Engineering, Illinois Institute of Technology, Chicago, IL 60616, USA. (e-mail: zhongqc@ieee.org).

The first gap comes from the structural constraint of the conventional UDE-based robust control [1]. The structural constraint states that, the lumped uncertainty should be "matched" with the control input, i.e., it should appear in the channel as the input. Otherwise, if the lumped uncertainty and control input are "mismatched", the tracking performance can not be guaranteed. In the state-space representation, the structural constraint always exists while the system order is two or higher. But for a first-order system, there is only one channel. The lumped uncertainty and control input are always "matched". The problem of structural constraint thus naturally disappears.

The second gap is that, the conventional UDE-based robust control belongs to full state feedback control, i.e., it requires all system states are available through measurements. But in many applications, only limited system states are available. Thus, there is a need to develop an output feedback version of the UDE-based robust control. In [9], a controller-observer structure is proposed by constructing a Luenberger-like state observer. This observer uses the lumped uncertainty estimation that comes from the UDE, and estimates the system states. However, the accuracy of states estimation directly depends on how accurate the lumped uncertainty estimation is, and vice versa. Thus, in this structure, the states estimation and lumped uncertainty estimation interact with each other. The preferred performance can be obtained only while the lumped uncertainty varies slowly. In a summary, the approach in [9] overcomes the second gap to some extent. But it has not addressed the first gap, i.e., the control input and lumped uncertainty should still be "matched".

To address the above two gaps simultaneously, the present paper proposes a UDE-based output feedback trajectory tracking control for a class of nonlinear SISO system, which is BIBO and Lipschitz smooth. The measured output of this system is also the controlled variable. The nonlinear system is first approximated by a proper first-order linear system, where the approximation error is viewed as a part of the lumped uncertainty term. The UDE is then adopted to estimate and compensate the lumped uncertainty term quickly. The proposed approach only uses the system output information, and does not rely on system modeling or identification. Compared to the aforementioned controller-observer structure, this approach can handle the uncertainties with high frequencies. And the structural constraint is also avoided.

In the following, the problem is formulated in Section II. Section III presents the main results. Here, the UDE-based output feedback trajectory tracking control is proposed, and,

the stability and robustness of the closed-loop system are analyzed. An experimental validation on a piezoelectric stage is presented in Section IV. Finally, Section V summarizes the concluding remarks.

II. Problem Formulation

The following SISO nonlinear system is considered,

$$\Sigma : \begin{array}{ll} \dot{x}(t) = & f(x(t), u(t)), \\ y(t) = & h(x(t), u(t)), \end{array} \tag{1}$$

where $x(t) \in \mathbb{R}^n$ is the state vector, $u(t) \in \mathbb{R}$, $y(t) \in \mathbb{R}$ are system input and output, respectively. $f(\cdot)$ is an unknown vector function, and $h(\cdot)$ is an unknown scalar function. The input-output relationship is denoted as $y(t) = \Sigma(u(t))$. Two assumptions are made for this system: 1) this system is assumed to be BIBO; 2) $\Sigma(\cdot)$ is assumed to be Lipschitz smooth.

The objective is to regulate the output $y(t)$ to the desired value $y_r(t) \in \mathbb{R}$. $y_r(t)$ is not necessary a continuous signal. Thus the following reference model is utilized to provide a continuous reference state $y_m(t) \in \mathbb{R}$.

$$\dot{y}_m(t) = -a_m y_m(t) + b_m y_r(t), \tag{2}$$

where a_m, $b_m > 0$. One can design a_m, b_m to guarantee that $y_m(t) = y_r(t)$ during the steady state, and $y_m(t)$ has a good transient performance. The control objective is to design $u(t)$ such that $y(t)$ tracks $y_m(t)$ fast and accurately. The following error dynamics is desired,

$$\dot{e}(t) = -ke(t), \tag{3}$$

where $e(t) = y_m(t) - y(t)$ denotes the tracking error, and $k > 0$ which guarantees $\lim_{t\to\infty} e(t) = 0$.

III. UDE-based Output Feedback Trajectory Tracking Control

A. Controller Derivation

As shown in Fig. 1, the input-output relationship is re-arranged after introducing a proper first-order linear system $\frac{b}{s+a}$, where $a > 0$, $b \neq 0$ and the sign of b should be the same as the sign of the system gain. The input-output relationship can be rewritten as

$$y(t) = \mathcal{L}^{-1}\left\{\frac{b}{s+a}\right\} * u(t) + z(t), \tag{4}$$

where "$*$" is the convolution operator, $\mathcal{L}^{-1}\{\cdot\}$ is the operator of inverse Laplace transform, and

$$z(t) = \Sigma(u(t)) - \mathcal{L}^{-1}\left\{\frac{b}{s+a}\right\} * u(t).$$

Accordingly, there is

$$\begin{array}{rcl} \dot{y}(t) & = & -ay(t) + bu(t) + \dot{z}(t) + az(t) \\ & = & -ay(t) + bu(t) + u_d(t), \end{array} \tag{5}$$

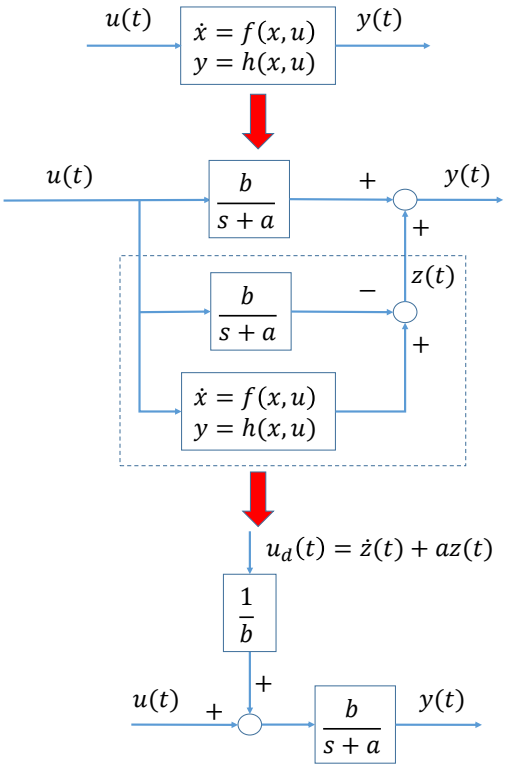

Figure 1. Equivalent transformation by introducing $\frac{b}{s+a}$.

where $u_d(t) = \dot{z}(t) + az(t)$ represents the lumped uncertainty term. Subtracting (5) from (2), there is

$$\begin{array}{rl} \dot{e}(t) = & -ke(t) + [ke(t) - a_m y_m(t) + b_m y_r(t) \\ & + ay(t) - bu(t) - u_d(t)], \end{array} \tag{6}$$

In order to achieve (3), the controller can be chosen as

$$u(t) = \frac{1}{b}\left[-a_m y_m(t) + b_m y_r(t) + ke(t) + ay(t) - u_d(t)\right]. \tag{7}$$

From (5), there is $u_d(t) = \dot{y}(t) + ay(t) - bu(t)$. Based on the idea of UDE-based robust control [1], a strictly proper and stable filter $G_f(s)$ is introduced, then $u_d(t)$ can be estimated as

$$\hat{u}_d(t) = g_f(t) * u_d(t) = g_f(t) * (\dot{y}(t) + ay(t) - bu(t)), \tag{8}$$

where $g_f(t) = \mathcal{L}^{-1}\{G_f(s)\}$ is the impulse response of $G_f(s)$. This filter has the unity gain and zero phase shift over the spectrum of $u_d(t)$, and zero gain elsewhere. Next, by replacing $u_d(t)$ in (7) with $\hat{u}_d(t)$ in (8), the UDE-based robust controller can be obtained as

$$\begin{array}{rl} u(t) = \frac{1}{b}\Bigg[& ay(t) - \mathcal{L}^{-1}\left\{\frac{sG_f(s)}{1 - G_f(s)}\right\} * y(t) + \\ & \mathcal{L}^{-1}\left\{\frac{1}{1 - G_f(s)}\right\} * (-a_m y_m(t) + b_m y_r(t) + ke(t))\Bigg]. \end{array} \tag{9}$$

The overall control scheme can be seen in Fig. 2.

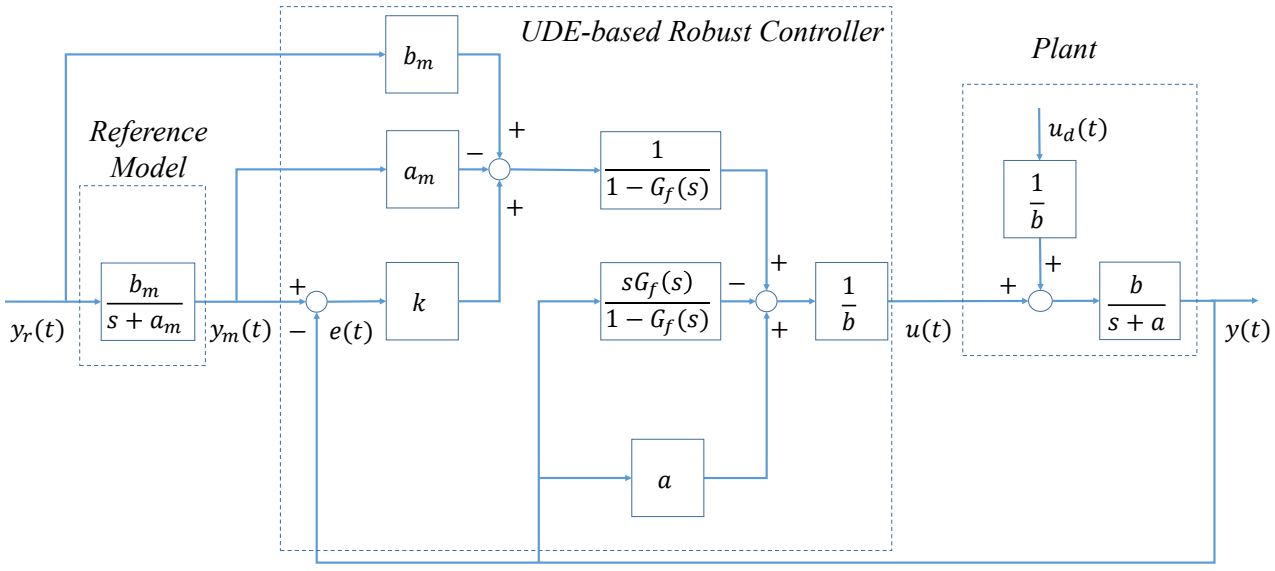

Figure 2. The block diagram of the proposed UDE-based robust output feedback control.

Remark 1. Under the ideal design of the filter $G_f(s)$, the UDE-based robust control guarantees that the tracking error asymptotically converge to 0, i.e., $\lim_{t\to\infty} e(t) = 0$. One practical choice of $G_f(s)$ is the first-order low-pass filter $G_f(s) = \frac{1}{T_f s+1}$, where T_f is the time constant, and is designed to provide a suitable bandwidth and an acceptable performance. In order to improve the performance, the internal model principle can be utilized in the design of $G_f(s)$, [11], [12]. As proposed in [11], the following filter can be used to handle a harmonic uncertainty term,

$$G_f(s) = 1 - \frac{s\prod_n (s^2 + (n\omega)^2)}{(s+\alpha)\prod_n (s^2 + \alpha_n s + \beta_n)}, \tag{10}$$

where $\omega = 2\pi f$, f is the frequency of reference state, n is the frequency multiplier, and α, α_n, β_n are design parameters. The proposed design could exactly guarantee that $G_f(s)$ has the unity gain and zero phase shift at the spectra $s = in\omega$.

B. BIBO Stability

Lemma 2. *If $\Sigma(u(t))$ satisfies the two assumptions in Section II, and the control input $u(t)$ is continuous and bounded by c, i.e., $\exists c > 0$ such that $\|u(t)\| \le c$, then, $u_d(t)$ in (5) is also bounded, i.e., $\exists M > 0$ such that $\|u_d(t)\| \le M$.*

Proof: Assume $b > 0$, the proof for $b < 0$ is similar. Based on the BIBO assumption of system (1), there exist non-negative constants γ_1 and γ_2, such that

$$\|y(t)\| = \|\Sigma(u(t))\| \le \gamma_1 \|u(t)\| + \gamma_2, \tag{11}$$

for all $\|u(t)\| \le c < \infty$. Define $\zeta(t) = \mathcal{L}^{-1}\left\{\frac{b}{s+a}\right\} * u(t)$, and it has the following solution

$$\zeta(t) = b\int_0^t e^{-a(t-\xi)} u(\xi) d\xi. \tag{12}$$

Furthermore, there is

$$\|\zeta(t)\| \le b\left(\int_0^t \left|e^{-a(t-\xi)}\right| d\xi\right)\left(\sup_{0<\xi<t} |u(\xi)|\right) \le \frac{bc}{a}. \tag{13}$$

Accordingly, it obtains that,

$$\begin{aligned}\|z(t)\| &= \|\Sigma(u(t)) - \zeta(t)\| \le \|\Sigma(u(t))\| + \|\zeta(t)\| \\ &\le \gamma_1 \|u(t)\| + \gamma_2 + \frac{bc}{a}.\end{aligned} \tag{14}$$

Moreover, since $\dot{\zeta}(t) = bu(t) - ab\int_0^t e^{-a(t-\zeta)} u(\zeta) d\zeta$, there is

$$\begin{aligned}\left\|\dot{\zeta}(t)\right\| &\le b\|u(t)\| + ab\left(\int_0^t \left|e^{-a(t-\xi)}\right| d\xi\right)\left(\sup_{0<\xi<t} |u(\xi)|\right) \\ &\le b\|u(t)\| + bc.\end{aligned} \tag{15}$$

Based on the assumption that $\Sigma(\cdot)$ is Lipschitz smooth, $\exists \gamma_3 \ge 0$ such that $\left\|\frac{d}{dt}\Sigma(u(t))\right\| \le \gamma_3$. Consequently,

$$\|\dot{z}(t)\| = \left\|\frac{d}{dt}\Sigma(u(t))\right\| + \left\|\dot{\zeta}(t)\right\| \le b\|u(t)\| + c + \gamma_3. \tag{16}$$

Combining (14), (15) and (16), it gives

$$\begin{aligned}\|u_d(t)\| &= \|\dot{z}(t) + az(t)\| \le \|\dot{z}(t)\| + a\|z(t)\| \\ &\le (b + a\gamma_1)\|u(t)\| + 2bc + \gamma_3 + a\gamma_2.\end{aligned} \tag{17}$$

Let $M = (b + a\gamma_1)\left(\sup_{0<\xi<t}|u(\xi)|\right) + 2bc + \gamma_3 + a\gamma_2$. $\|u_d(t)\|$ is then bounded by M. This completes the proof. ■

Theorem 3. *The overall closed-loop system, which consists of (1), (2) and (9), is BIBO stable.*

Proof: After rearranging the blocks in Fig. 2, the closed-loop system can be expressed as the form in Fig. 3, where

$$G_1(s) = \frac{b_m\,(s+k)}{s+a_m}, \tag{18}$$

$$G_2(s) = \frac{1}{b(1-G_f(s))}, \tag{19}$$

$$G_3(s) = (k-a)+(s+a)\,G_f(s). \tag{20}$$

The stability of the system depends on the roots of the characteristic equation,

$$1+\frac{b}{s+a}G_2(s)G_3(s)=0. \tag{21}$$

Applying (19) and (20) into (21) results in $s+k=0$. Obviously, its root locates at $s=-k<0$, which is on the open left-half of the complex plane. It can be seen that the filter $G_f(s)$ does not affect the location of the pole, and only k affects the stability. The BIBO stability is then proved. ■

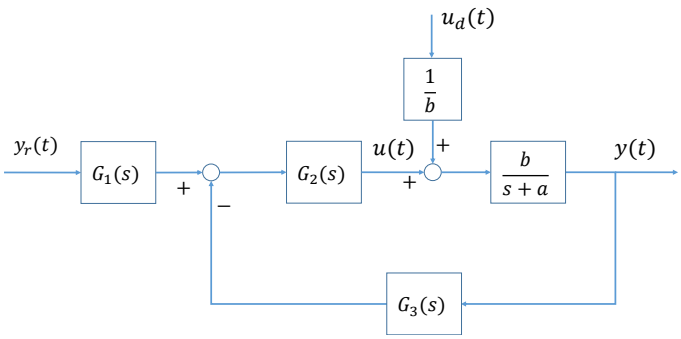

Figure 3. Equivalent representation of the UDE-based robust control for analysis.

Proposition 4. *If $y_r(t)$ is a bounded signal, then all of signals in the closed-loop system shown in Fig. 3 are bounded.*

Proof: According to Theorem 3, the output $y(t)$ is bounded while $y_r(t)$ is bounded. Since the controller (9) is a continuous function of $y(t)$ and $y_r(t)$, $u(t)$ is bounded. Consequently, $u_d(t)$ is also bounded based on Lemma 2. ■

Remark 5. The choice of parameters in the first-order linear system $\frac{b}{s+a}$ are elaborated as follows. The bandwidth a is chosen to cover the frequency of $y_r(t)$, the parameter b is then chosen to make the ratio b/a greater than the static gain of the original nonlinear system $y(t)=\Sigma(u(t))$.

C. Robustness Performance

In the following, the capitalized variables are the Laplace transform for the time varying variables, e.g., $Y(s)$, $U_d(s)$ are the Laplace transforms of $y(t)$ and $u_d(t)$, respectively. The performance of trajectory tracking and disturbance rejection can be obtained through the following transfer functions,

$$H_m(s)=\frac{\frac{b}{s+a}G_2(s)G_1(s)}{1+\frac{b}{s+a}G_2(s)G_3(s)}=\frac{b_m}{s+a_m}, \tag{22}$$

$$H_d(s)=\frac{\frac{1}{s+a}}{1+\frac{b}{s+a}G_2(s)G_3(s)}=\frac{1-G_f(s)}{s+k}, \tag{23}$$

where $H_m(s)$ is the transfer function form $Y_r(s)$ to $Y(s)$, $H_d(s)$ is the transfer function from $U_d(s)$ to $Y(s)$. Thus in the frequency domain, there is

$$Y(s)=H_m(s)Y_r(s)+H_d(s)U_d(s). \tag{24}$$

Here, $H_m(s)$ is the transfer function of reference model (2), i.e., $Y_m(s)=H_m(s)Y_r(s)$. It is seen that $Y(s)$ is dominated by the reference state $Y_m(s)$, and perturbed by the uncertainty term $U_d(s)$. The trajectory tracking is directly determined by the reference model, and the disturbance rejection is ruled by designing $G_f(s)$ and k simultaneously. The smaller the magnitude of $\|H_d(s)\|_{dB}$ is, the better disturbance rejection performance can be obtained. If the spectrum of the uncertainty $u_d(t)$ is $[\omega_1,\omega_2]$, and the required tolerance of the disturbance attenuation is $\delta>0$, then the design should guarantee that

$$\|H_d(i\omega)\|_{dB}\le 20\log\delta,\ \forall\omega\in[\omega_1,\omega_2]\,. \tag{25}$$

Since $G_f(s)$ is designed as a low-pass filter with a bandwidth ω_H, $1-G_f(s)$ is thus a high-pass filter with bandwidth ω_H. $\frac{1}{s+k}$ is meanwhile a low-pass filter with bandwidth $\omega_L=k$. ω_L and ω_H are properly selected to satisfy the condition (25).

D. Asymptotic Convergence of Tracking Error

Theorem 6. *Consider the overall closed-loop system which consists of (1), (2) and (9), and $G_f(s)$ is designed as in (10). The tracking error $e(t)$ asymptotically converges to* 0.

Proof: In the frequency domain, the system (5) becomes

$$sY(s)=-aY(s)+bU(s)+U_d(s), \tag{26}$$

the reference model (2) becomes

$$sY_m(s)=-a_mY_m(s)+b_mY_r(s), \tag{27}$$

and the controller (9) becomes

$$bU(s)=-a_mY_m(s)+b_mY_r(s)+kE(s)+aY(s) - U_d(s)G_f(s). \tag{28}$$

Combining (26), (27) and (28), there is

$$sE(s)=-kE(s)-U_d(s)\,[1-G_f(s)]\,. \tag{29}$$

Therefore, the tracking error is

$$E(s)=-\frac{1}{s+k}\,[1-G_f(s)]\,U_d(s). \tag{30}$$

One can decompose $U_d(s)=\frac{P_2(s)}{P_1(s)N_i(s)}$, where $N_i(s)$ is the internal model of $U_d(s)$, and $P_1(s)$, $P_2(s)$ are proper and Hurwitz polynomials. As shown in (10), $1-G_f(s)=\frac{N_i(s)}{P_3(s)}$, which is strictly proper and stable, and $P_3(s)$ is a Hurwitz polynomial. Therefore, $\lim_{s\to0}[1-G_f(s)]\,U_d(s)=\lim_{s\to0}\frac{P_2(s)}{P_1(s)P_3(s)}$ is a constant value. By applying the final value theorem to (30), there is

$$\lim_{t\to\infty}e(t)=\lim_{s\to0}sE(s)=-\lim_{s\to0}\frac{sU_d(s)}{s+k}\,[1-G_f(s)]=0,$$

which indicates the asymptotic convergence of tracking error. This completes the proof. ■

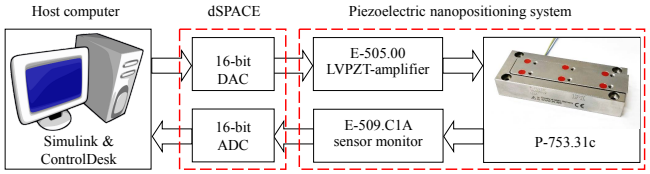

Figure 4. Experimental setup of Physik Instrumente P-753.31c nanopositioning system.

IV. Experimental Validation

A. Experimental Setup and Modeling of Piezoelectric Stage

The experimental setup is shown in Fig. 4, which consists of a piezoelectric stage P-753.31c, a linear voltage amplifier E-505.00, a sensor monitor E-509.C1A KG, a dSPACE-DS1104 board, and a host computer. The sampling time is $0.01ms$, and the hardware resolution is around $0.0012\mu m$.

The hysteresis effect in this system is rate-dependent. To verify this fact, several sinusoidal signals with different frequencies are used as input signals to obtain a series of major hysteresis loops. Specifically, the input signals are selected as $u(t) = 3(\sin(2\pi ft) + 1)V$ with the frequencies $f = 1Hz,\ 50Hz,\ 100Hz$. The resulting hysteresis loops are shown in Fig. 5. As seen, there is a marked increase in hysteresis while using higher frequencies. $y = k_s u$ is the approximate symmetry axis of hysteresis loops.

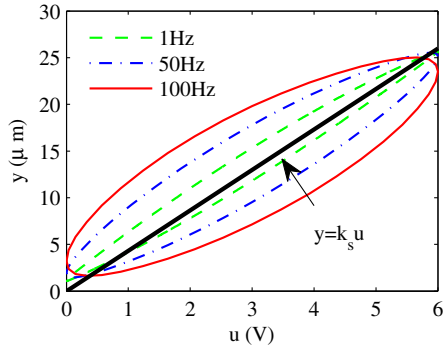

Figure 5. Major hysteresis loops of P-753.31c piezoelectric system resulted from sinusoidal signals with different frequencies. u is the input voltage and y is the output displacement.

To characterize the rate-dependent hysteresis, different models have been proposed in [13], [14], [15], [16]. In this paper, the piezoelectric stage is assumed to be described by the rate-dependent Prandtl-Ishlinskii hysteresis model in [13], since this model has been successfully used for the modeling of rate-dependent hysteresis in a piezoelectric system. To formulate the rate-dependent Prandtl-Ishlinskii hysteresis model, the rate-dependent play operator, $w(t) = F_{r_i(\dot{u})}[u](t) = f_{r_i(\dot{u})}(u(t),\ F_{r_i(\dot{u})}[u](t_{j-1}))$, with dynamic threshold $r_i(\dot{u}) > 0$, is defined as

$$
\begin{aligned}
&F_{r_i(\dot{u})}[u](0) = f_{r_i(\dot{u})}(u(0),\ 0),\\
&f_{r_i(\dot{u})}(u,\ w(t_{j-1})) =\\
&\begin{cases}
\max(u(t) - r_i(\dot{u}), w(t_{j-1})), & u(t) > u(t_{j-1})\\
\min(u(t) + r_i(\dot{u}), w(t_{j-1})), & u(t) < u(t_{j-1})\\
w(t_{j-1}), & u(t) = u(t_{j-1})
\end{cases}\\
&\text{for } t_{j-1} < t \le t_j \text{ and } 1 \le j \le \bar{M}, \qquad (31)
\end{aligned}
$$

where $u(t) \in AC[0,\ t_E]$ is the input voltage, with $AC[0,\ t_E]$ denoting the space of absolutely continuous functions on time interval $[0,\ t_E]$. $0 = t_0 < t_1 < \cdots < t_{\bar{M}} = t_E$ is partition of $[0,\ t_E]$, and that the function $u(t)$ is monotone on each of the sub-intervals $(t_j,\ t_{j+1}]$. The argument of the operator is written in square brackets to indicate the functional dependence, since it maps a function to a function. Then, similar to the rate-independent Prandtl-Ishlinskii hysteresis model that is constructed via the superposition of weighted play operators with different thresholds, the rate-dependent Prandtl-Ishlinskii model is formulated as following [13],

$$y(t) = H[u](t) = a_0 u(t) + \sum_{i=1}^{N} a_i F_{r_i(\dot{u})}[u](t), \qquad (32)$$

where $y(t)$ is the system output displacement, $a_i,\ i = 0,\ 1,\ 2, \cdots,\ N$ are positive weights, and N is the total number of rate-dependent play operators. It should be noted that the dynamic thresholds $r_i(\dot{u})$ should satisfy $0 \le r_1(\dot{u}) \le r_2(\dot{u}) \le \cdots \le r_N(\dot{u})$. Specifically, $r_i(\dot{u}) = \alpha_i + g(\dot{u}) = \zeta i + \beta|\dot{u}|$ from [13] will be used in this paper.

Furthermore, the system (32) satisfies the two assumptions mentioned in previous section. Due to the page limits, the proof is omitted.

B. Control Design

The controller design does not use the information of system (32). The reference trajectory is $y_r(t) = 1 + \sin(\omega t - \pi/2)\mu m$, where $\omega = 2\pi f$ represents the operating frequency of the piezoelectric stage. The reference model (2) is selected as $\frac{b_m}{s+a_m} = \frac{\omega_M}{s+\omega_M}$ with $a_m = b_m = \omega_M$. And its bandwidth $\omega_M = 50000\pi$. The first-order system is chosen as $\frac{b}{s+a}$, where $a = 60000\pi$ and $b = 260000\pi$. Since there is only one major frequency, $n = 1$ in (10), and the filter $G_f(s)$ becomes the following form,

$$G_f(s) = 1 - \frac{s(s^2 + \omega^2)}{(s+\alpha)(s^2 + \alpha_1 s + \beta_1)}. \qquad (33)$$

Specifically, the parameters are chosen as $\alpha = 1000$, $\alpha_1 = 1800\pi$ and $\beta_1 = 810000\pi^2$. Let the tolerance of disturbance attenuation is $\delta = 0.000001$, then the condition must be $\|H_d(i\omega)\|_{dB} \le 20\log\delta = -120dB$. The error feedback gain is chosen as $k = 200000$. The controller is designed as (9).

C. Experimental Results

As shown in Fig. 6, the tracking performances for $f = 100Hz$ and $f = 1100Hz$ are presented. The root-mean-square (RMS) values are $0.0033\mu m$ while $f = 100Hz$, and

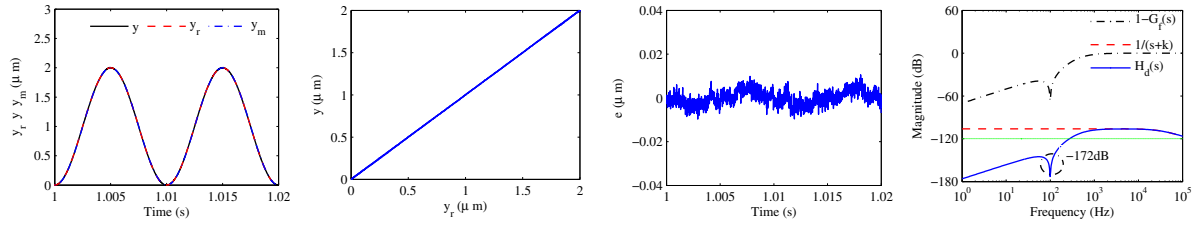

$(a)\ f = 100Hz$

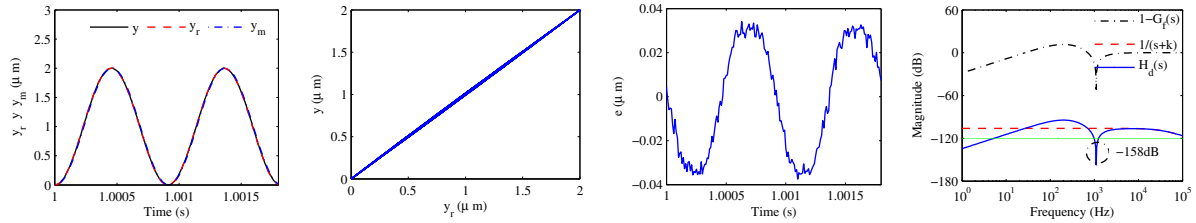

$(b)\ f = 1100Hz$

Figure 6. Results of tracking sinusoidal signals. 1st column: Output; 2nd column: Compensated hysteresis loop; 3rd column: Tracking error; 4th column: Bode plots of $1 - G_f(s)$, $\frac{1}{s+k}$, and $H_d(s)$.

$0.0222\mu m$ while $f = 1100Hz$. The insight of $100Hz$ has a smaller tracking error than $1100Hz$ can be revealed from the Bode plots in the 4th column of Fig. 6. Since the magnitude of $H_d(s)$ is smaller at $100Hz$, its tracking performance is better. The internal model embedded design of $G_f(s)$ in (33) can be utilized to reduce the magnitude of $H_d(s)$ at $1100Hz$. At $1100Hz$, the relative maximum absolute error (RMA) is around 1.7%. Therefore, a fine tracking is achieved at a high frequency, $1100Hz$, which is 37.93% of the lowest resonant frequency, a significant improvement compared to the commercially available range at $1\% - 10\%$.

V. Conclusion

The proposed approach has extended the conventional UDE-based robust control to an output feedback version, and relaxed the structural constraint. The robustness analysis revealed that the tracking performance is determined by $\|H_d(s)\|_{dB}$. Accordingly, the internal model principle was utilized in the filter design of UDE to enhance the tracking performance. An experimental study on a piezoelectric nanopositioning system was conducted to show the practical implementation, which demonstrated the effectiveness of the proposed control.

References

[1] Q.-C. Zhong and D. Rees, "Control of uncertain LTI systems based on an uncertainty and disturbance estimator," *ASME Trans. J. Dyn. Sys. Meas. Control*, vol. 126, no. 4, pp. 905–910, Dec. 2004.

[2] J. Chen, B. Ren, and Q.-C. Zhong, "UDE-based trajectory tracking control of piezoelectric stages," *IEEE Trans. Ind. Electron.*, vol. 63, no. 10, pp. 6450–6459, Oct 2016.

[3] B. Ren, Y. Wang, and Q.-C. Zhong, "UDE-based control of variable-speed wind turbine systems," *International Journal of Control*, vol. 90, no. 1, pp. 121–136, Jan. 2017.

[4] I. Aharon, D. Shmilovitz, and A. Kuperman, "Robust output voltage control of multimode non-inverting DC–DC converter," *International Journal of Control*, pp. 1–11, Dec. 2015.

[5] Y. Wang, B. Ren, and Q.-C. Zhong, "Robust power flow control of grid-connected inverters," *IEEE Trans. Ind. Electron.*, vol. 63, no. 11, pp. 6887–6897, Nov. 2016.

[6] Q.-C. Zhong, Y. Wang, and B. Ren, "UDE-based robust droop control of inverters in parallel operation," *IEEE Trans. Ind. Electron.*, vol. 64, no. 9, pp. 7552–7562, Sept. 2017.

[7] L. Sun, D. Li, Q. C. Zhong, and K. Y. Lee, "Control of a class of industrial processes with time delay based on a modified uncertainty and disturbance estimator," *IEEE Trans. Ind. Electron.*, vol. 63, no. 11, pp. 7018–7028, Nov. 2016.

[8] R. Sanz, P. Garcia, Q. C. Zhong, and P. Albertos, "Predictor-based control of a class of time-delay systems and its application to quadrotors," *IEEE Trans. Ind. Electron.*, vol. 64, no. 1, pp. 459–469, Jan 2017.

[9] S. Talole, T. Chandar, and J. P. Kolhe, "Design and experimental validation of ude based controller–observer structure for robust input–output linearisation," *International Journal of Control*, vol. 84, no. 5, pp. 969–984, Jun. 2011.

[10] Q.-C. Zhong, A. Kuperman, and R. Stobart, "Design of UDE-based controllers from their two-degree-of-freedom nature," *International Journal of Robust and Nonlinear Control*, vol. 21, pp. 1994–2008, Nov. 2011.

[11] B. Ren, Q.-C. Zhong, and J. Dai, "Asymptotic reference tracking and disturbance rejection of UDE-based robust control," *IEEE Trans. Ind. Electron.*, vol. 64, no. 4, pp. 3166–3176, Apr. 2017.

[12] B. A. Francis and W. M. Wonham, "The internal model principle of control theory," *Automatica*, vol. 12, no. 5, pp. 457–465, Sept. 1976.

[13] M. Al Janaideh and P. Krejci, "Inverse rate-dependent Prandtl–Ishlinskii model for feedforward compensation of hysteresis in a piezomicropositioning actuator," *IEEE/ASME Trans. Mechatronics*, vol. 18, no. 5, pp. 1498–1507, Oct. 2013.

[14] M. Al Janaideh, S. Rakheja, and C.-Y. Su, "Experimental characterization and modeling of rate-dependent hysteresis of a piezoceramic actuator," *Mechatronics*, vol. 19, no. 5, pp. 656–670, Aug. 2009.

[15] R. Ben Mrad and H. Hu, "A model for voltage-to-displacement dynamics in piezoceramic actuators subject to dynamic-voltage excitations," *IEEE/ASME Trans. Mechatronics*, vol. 7, no. 4, pp. 479–489, Dec. 2002.

[16] G. Gu and L. Zhu, "Modeling of rate-dependent hysteresis in piezoelectric actuators using a family of ellipses," *Sens. Actuators A, Phys.*, vol. 165, no. 2, pp. 303–309, Feb. 2011.